## ACKNOWLEDGMENTS

We thank the family for their co-operation. This study was supported by the Health and Labour Research Grants in 2009 by Ministry of Health, Labour and Welfare in Japan.

## REFERENCES

Holm VA, Cassidy SB, Butler MG. 1993. Prader–Willi syndrome: Consensus diagnostic criteria. Pediatrics 91:398–402.

Kurotaki N, Imaizumi K, Harada N, Masuno M, Kondoh T, Nagai T, Ohashi H, Naritomi K, Tsukahara M, Makita Y, Sugimoto T, Sonoda T, Hasegawa T, Chinen Y, Tomita Ha HA, Kinoshita A, Mizuguchi A, Yoshiura T, Ki K, Ohta T, Kishino T, Fukushima Y, Niikawa N, Matsumoto N. 2002. Haploinsufficiency of NSD1 causes Sotos syndrome. Nat Genet 30:365–366.

Kurotaki N, Stankiewicz P, Wakui K, Niikawa N, Lupski JR. 2005. Sotos syndrome common deletion is mediated by directly oriented subunits within inverted Sos-REP low-copy repeats. Hum Mol Genet 14:535–542.

Ledbetter DH, Riccardi VM, Airhart SD. 1981. Deletion of chromosome 15 as a cause of Prader–Willi syndrome. N Engl J Med 304:325–329.

Miyake N, Kurotaki N, Sugawara H, Shimokawa O, Harada N, Kondoh T, Tsukahara M, Ishikiriyama S, Sonoda T, Miyoshi Y, Sakazume S, Fukushima Y, Ohashi H, Nagai T, Kawame H, Kurosawa K, Touyama M, Shiihara T, Okamoto N, Nishimoto J, Yoshiura K, Ohta T, Kishino T, Niikawa N, Matsumoto N. 2003. Preferential paternal origin of microdeletions caused by prezygotic chromosome or chromatid rearrangements in Sotos syndrome. Am J Hum Genet 72:1331–1337.

Nagai T, Matsuo N, Kayanuma Y, Tonoki H, Fukushima Y, Ohashi H, Murai T, Hasegawa T, Kuroki Y, Niikawa N. 2000. Standard growth curves for Japanese patients with Prader–Willi syndrome. Am J Med Genet 95:130–134.

Nagai T, Matsumoto N, Kurotaki N, Harada N, Niikawa N, Ogata T, Imaizumi K, Kurosawa K, Kondoh T, Ohashi H, Tsukahara M, Makita Y, Sugimoto T, Sonoda T, Yokoyama T, Uetake K, Sakazume S, Fukushima Y, Naritomi K. 2003. Sotos syndrome and haploinsufficiency of NSD1: Clinical features of intragenic mutations and submicroscopic deletions. J Med Genet 40:285–289.

Sahoo T, del Gaudio D, German JR, Shinawi M, Peters SU, Person RE, Garnica A, Cheung SW, Beaudet AL. 2008. Prader–Willi phenotype caused by paternal deficiency for the HBII-85 C/D box small nucleolar RNA cluster. Nat Genet 40:719–721.

Shimojima K, Páez MT, Kurosawa K, Yamamoto T. 2009. Proximal interstitial 1p36 deletion syndrome: The most proximal 3.5-Mb microdeletion identified on a dysmorphic and mentally retarded patient with inv(3)(p14.1q26.2). Brain Dev 31:629–633.

Visser R, Shimokawa O, Harada N, Kinoshita A, Ohta T, Niikawa N, Matsumoto N. 2005. Identification of a 3.0-kb major recombination hotspot in patients with Sotos syndrome who carry a common 1.9-Mb microdeletion. Am J Hum Genet 76:52–67.

# ARTICLE

# *SMOC1* Is Essential for Ocular and Limb Development in Humans and Mice

Ippei Okada,[1,14] Haruka Hamanoue,[1,2,14] Koji Terada,[3] Takaya Tohma,[4] Andre Megarbane,[5] Eliane Chouery,[5] Joelle Abou-Ghoch,[5] Nadine Jalkh,[5] Ozgur Cogulu,[6] Ferda Ozkinay,[6] Kyoji Horie,[7] Junji Takeda,[7,8] Tatsuya Furuichi,[9,10] Shiro Ikegawa,[9] Kiyomi Nishiyama,[1] Satoko Miyatake,[1] Akira Nishimura,[1] Takeshi Mizuguchi,[1,15] Norio Niikawa,[11,12] Fumiki Hirahara,[2] Tadashi Kaname,[13] Koh-ichiro Yoshiura,[12] Yoshinori Tsurusaki,[1] Hiroshi Doi,[1] Noriko Miyake,[1] Takahisa Furukawa,[3] Naomichi Matsumoto,[1,*] and Hirotomo Saitsu[1,*]

Microphthalmia with limb anomalies (MLA) is a rare autosomal-recessive disorder, presenting with anophthalmia or microphthalmia and hand and/or foot malformation. We mapped the MLA locus to 14q24 and successfully identified three homozygous (one nonsense and two splice site) mutations in the SPARC (secreted protein acidic and rich in cysteine)-related modular calcium binding 1 (*SMOC1*) in three families. *Smoc1* is expressed in the developing optic stalk, ventral optic cup, and limbs of mouse embryos. *Smoc1* null mice recapitulated MLA phenotypes, including aplasia or hypoplasia of optic nerves, hypoplastic fibula and bowed tibia, and syndactyly in limbs. A thinned and irregular ganglion cell layer and atrophy of the anteroventral part of the retina were also observed. Soft tissue syndactyly, resulting from inhibited apoptosis, was related to disturbed expression of genes involved in BMP signaling in the interdigital mesenchyme. Our findings indicate that SMOC1/Smoc1 is essential for ocular and limb development in both humans and mice.

## Introduction

Microphthalmia with limb anomalies (MLA [MIM 206920]), also known as Waardenburg anophthalmia syndrome or ophthalmoacromelic syndrome, is a rare autosomal-recessive disorder first described by Waardenburg.[1] It is characterized by ocular anomalies ranging from mild microphthalmia to true anophthalmia and by limb anomalies such as oligodactyly, syndactyly, and synostosis of the 4th and 5th metacarpals.[2–4] The genetic cause for MLA has remained unknown.

It is widely known that secreted signaling molecules such as Sonic hedgehog (Shh), wingless-type MMTV integration site family (Wnt), transforming growth factor β (Tgf-β), bone morphogenetic proteins (Bmps), and fibroblast growth factor (Fgf) are involved in the development of many organs and tissues, including the eyes and limbs.[5,6] In particular, mutations in *BMP4* (MIM 112262) have resulted in anophthalmia with systemic manifestations, including polydactyly and/or syndactyly (also known as micropthalmia, syndromic 6, MCOPS6 [MIM 607932]),[7] highlighting importance of BMP signaling in both the developing eye and limb.

*SMOC1* (MIM 608488), which encodes SPARC (secreted protein acidic and rich in cysteine)-related modular calcium binding 1, is a member of the SPARC (also known as BM-40) matricellular protein family that modulates cell-matrix interaction by binding to many cell-surface receptors, the extracellular matrix, growth factors, and cytokines.[8,9] SMOCs are extracellular glycoproteins with five domains: an N-terminal follistatin-like (FS) domain, two thyroglobulin-like (TY) domains, a domain unique to SMOC, and an extracellular calcium-binding (EC) domain.[9] SMOC1 is widely expressed in various tissues with localization to basement membranes.[9,10] Although the biological function of SMOC1 remains largely unknown, it has been recently reported that *Xenopus* smoc protein, the ortholog of human SMOC1, acts as a BMP antagonist,[11] suggesting that human SMOC1 can also modulate BMP signaling.

Here, we demonstrate that *SMOC1* mutations cause MLA. We also show that *Smoc1* null mice recapitulated

[1]Department of Human Genetics, Yokohama City University Graduate School of Medicine, 3-9 Fukuura, Kanazawa-ku, Yokohama 236-0004, Japan; [2]Department of Obstetrics and Gynecology, Yokohama City University Graduate School of Medicine, 3-9 Fukuura, Kanazawa-ku, Yokohama 236-0004, Japan; [3]Department of Developmental Biology, Osaka Bioscience Institute, 6-2-4 Furuedai, Suita, Osaka 565-0874, Japan; [4]Division of Pediatrics, Okinawa Prefectural Nanbu Medical Center & Children's Medical Center, 118-1 Ikyoku, Arakawa, Haebaru, Okinawa 901-1193, Japan; [5]Medical Genetics Unit, St. Joseph University, Beirut 1104-2020, Lebanon; [6]Department of Pediatrics, Ege University Faculty of Medicine, 35100 Bornova-Izmir, Turkey; [7]Department of Social and Environmental Medicine, Graduate School of Medicine, Osaka University, 2-2 Yamadaoka, Suita, Osaka 565-0871, Japan; [8]Center for Advanced Science and Innovation, Osaka University, 2-1 Yamadaoka, Suita, Osaka 565-0871, Japan; [9]Laboratory for Bone and Joint Disease, Center for Genomic Medicine, RIKEN, 4-6-1 Shirokanedai, Minato-ku, Tokyo 108-8639, Japan; [10]Laboratory Animal Facility, Research Center for Medical Sciences, Jikei University School of Medicine, 3-25-8, Nishi-Shimbashi, Minato-ku, Tokyo 105-8461, Japan; [11]Research Institute of Personalized Health Sciences, Health Sciences University of Hokkaido, Ishikari-Tobetsu, Hokkaido 061-0293, Japan; [12]Department of Human Genetics, Nagasaki University Graduate School of Biomedical Sciences, Sakamoto 1-12-4, Nagasaki 852-8523, Japan; [13]Department of Medical Genetics, University of the Ryukyus Faculty of Medicine, 207 Uehara, Nishihara, Okinawa 903-0215, Japan

[14]These authors contributed equally to this work

[15]Current address: Laboratory of Biochemistry and Molecular Biology, National Cancer Institute, National Institutes of Health, Building 37, Room 6050, Bethesda, MD 20892, USA

*Correspondence: naomat@yokohama-cu.ac.jp (N.M.), hsaitsu@yokohama-cu.ac.jp (H.S.)

DOI 10.1016/j.ajhg.2010.11.012. 

MLA phenotypes, indicating that *SMOC1* plays essential roles in both eye and limb development in humans and mice.

## Subjects and Methods

### Subjects

A total of four families with one or two cases of MLA were analyzed in this study, including three previously reported families (A, B, and C).[12,13] Family X from Turkey, which has been previously described,[14] was newly recruited to this study. Detailed clinical information of all the patients is available in the literature,[12,14] and phenotypes of patients with confirmed mutations are summarized in Table S1 (available online). A total of five affected and 16 unaffected members from the four families were analyzed in the linkage study. Genomic DNA was obtained from peripheral-blood leukocytes with the use of QuickGene 610-L (Fujifilm, Tokyo, Japan) after informed consent had been given. Experimental protocols were approved by the institutional review board of Yokohama City University School of Medicine.

### SNP Genotyping, and Fine Mapping with Short Tandem Repeat Markers

Whole-genome SNP genotyping, with the use of GeneChip Human Mapping 50K Array XbaI (Affymetrix, Santa Clara, CA), and fine mapping of possible candidate regions, with the use of additional microsatellite markers, were performed as previously described.[12,15] The list of primers used for fine mapping is presented in Table S2.

### Linkage Analysis

Multipoint linkage analyses using aligned SNPs were performed with ALLEGRO software.[16] Two-point linkage analyses of candidate regions were performed with the LINKAGE package MLINK (FASTLINK software, version 5.1). In each program, an autosomal-recessive model of inheritance with complete penetrance and a disease-allele frequency of 0.001 were applied.

### Mutation Analysis of Candidate Genes

All coding exons and exon-intron boundaries of *RAD51L1* (MIM 602948), *ACTN1* (MIM 102575), *ERH* (MIM 601191), *SRSF5* (MIM 600914), *DCAF5* (MIM 603812), *COX16*, *EXD2*, *GALNTL1*, *SLC39A9*, *KIAA0247*, *MED6* (MIM 602984), *TTC9* (MIM 610488), *MAP3K9* (MIM 600136), and *SMOC1* (transcript variant 1, GenBank accession number NM_001034852.1) were analyzed in the probands of families A, C, and X. The transcript variant 2 of *SMOC1* (GenBank accession number NM_022137.4) is 3 bp shorter than the variant 1, leading to an in-frame amino acid deletion at position 431. PCR was cycled 35 times at 94°C for 30 s, at 60°C for 30 s, and at 72°C for 30–90 s in a total volume of 20 μl containing 30 ng genomic DNA as a template, 0.5 μM forward and reverse primers, 200 μM each deoxyribonucleotide triphosphate (dNTP), 1 × ExTaq buffer, and 0.25 U ExTaq (Takara). All primers were designed with Primer3 software. Detailed information of primers is available upon request. PCR products were purified with ExoSAP (USB) and sequenced with BigDye Terminator 3.1 (Applied Biosystems) on a 3100 Genetic Analyzer. Sequences of patients were compared to reference genome sequences in the UCSC Genome Browser (February 2009 assembly) with Seqscape software, version 2.1 (Applied Biosystems).

### Animals

*Smoc1* mutant mice, created with the use of the *Sleeping Beauty* transposon system, have been previously described.[17] Line PV384 was provided by the RIKEN BioResource Center through the National BioResource Project of MEXT, Japan. Three independent mouse lines (no. 1 to no. 3), each with a single insertion in intron 1 of *Smoc1*, were bred as heterozygotes. Lines 1 and 3 were backcrossed for at least four generations to a C57BL/6J background. Line 2 was maintained with a mixed background of C57BL/6J and ICR. We mainly analyzed line 1, but we confirmed similar phenotypes in lines 2 and 3. Animals were housed in accordance with protocols approved by the Institutional Animal Care and Use Committee at Yokohama City University, School of Medicine. PCR genotyping of mice was performed with the use of genomic DNA from yolk-sac, ear, or tail biopsies. The following primers were used: PV384-WF, 5′-AAAGGCTGGGAATTGTTTG A-3′; PV384-WR, 5′-TGCAGCTGAAACTGTCTCTCC-3′; PV384-MF, 5′-TGTCCTAACTGACTTGCCAAA-3′. The PV384-WF/PV384-WR primers amplified a 441 bp wild-type (WT) product, and the PV384-MF/PV384-WR primers amplified a 218 bp mutant product.

### Southern Hybridization

Genomic DNA was extracted from livers or tail biopsies of PV384 heterozygous ($Smoc1^{Tp/+}$) mice via standard protocols. The gene-trap insertions were analyzed by Southern hybridization with the use of 10 μg of *Sac*I-, *Nde*I-, BglII-, and *Eco*RI-digested DNA. The probe (451 bp), which hybridized to the internal ribosome entry site (IRES) in the gene-trap vector, was synthesized with the DIG PCR Probe Synthesis Kit (Roche) with the use of the following primers: 5′-CTAACGTTACTGGCCGAAGC-3′ and 5′-CCCAGATCAGATCCCATACAA-3′. Hybridization, washing, and detection of probes were performed according to the manufacturer's protocol. Images were captured with the FluorChem system (Alpha Innotech).

### Cloning of Gene-Trap Insertion Sites

After identification of aberrant DNA fragments by Southern hybridization, *Nde*I-, *Sac*I-, and *Eco*RI-digested DNA from PV384 mice was fractionated by electrophoresis, and appropriately sized fragments containing *Ol1* (*other locus 1*), *Ol2*, and *Ol3* were isolated with a QIAEXII Gel Extraction Kit (QIAGEN). The isolated DNA was self-ligated by Ligation High ver.2 (Toyobo), precipitated with ethanol, and dissolved in 20 μl EB buffer (QIAGEN). Inverse PCR was performed in 25 μl reactions, containing 2 μl ligated DNA, 1 × PCR buffer for KOD FX, 0.4 mM each dNTP, 0.5 μM each primer, and 0.5 U KOD FX DNA polymerase (Toyobo). Primers common to *Ol1*, *Ol2*, and *Ol3* were as follows: Inv-F, 5′- AT CGCCAGTTCTGTATGAACGGTCTGGTCTT-3′; Inv-R, 5′-CCCTC TTTACGTGCCAGCCATCTTAGAGATAC-3′. Confirmatory PCR of gene-trap insertion sites for *Ol1*, *Ol2*, and *Ol3* loci was performed with the use of the following primers: *Ol1*-F, 5′-GAGTGGTATTCA TTGGATTCTGCTGAT-3′; *Ol2*-F, 5′-AAATCCAGCTGGCCAACAGA CTAAG-3′; *Ol3*-F, 5′-TTGCCGGGTAGACTCTATCAAGAACCA-3′; TBAL-R, 5′-CTTGTGTCATGCACAAAGTAGATGTCC-3′. Primer sets of *Ol1*-F/TBAL-R, *Ol2*-F/TBAL-R, and *Ol3*-F/TBAL-R could amplify 175 bp, 607 bp, and 767 bp products, respectively. These PCR primer pairs were also used for genotyping of mice harboring a single insertion at the *Smoc1* locus.

### Confirmation of Promoter- and Poly(A)-Trapped Transcripts

Whole embryos at embryonic day 10.5 (E10.5) and E11.5 were stored in RNAlater solution (QIAGEN). Total RNA was extracted from WT, *Smoc1*$^{Tp/+}$, and *Smoc1*$^{Tp/Tp}$ embryos with the use of RNeasy Plus Mini (QIAGEN). One microgram total RNA was subjected to reverse transcription with the use of a PrimeScript 1$^{st}$ Strand Synthesis Kit with random hexamers (Takara). A control reaction with no reverse transcriptase was included in each experiment. PCR was performed in 20 μl reactions, containing 1 μl cDNA, 1 × PCR Buffer for KOD FX, 0.4 mM each dNTP, 0.3 μM each primer, and 0.4 U KOD FX (Toyobo). Primers used are listed below: *Smoc1*-F, 5′-GTCCCCACCTCCCCAAGTGCTTTGA-3′; *LacZ*-R, 5′-TGCCAAAAGACGGCAATATGGTGGAAA-3′; *GFP*-F, 5′-TCACATGGTCCTGCTGGAGTTCGTGAC-3′; *Smoc1*-R, 5′-ACACTTGCTCTGGCCAGCATCTTTGCAT-3′. Primer sets of *Smoc1*-F/*Smoc1*-R, *Smoc1*-F/*LacZ*-R, and *GFP*-F/*Smoc1*-R could amplify native *Smoc1* (366 bp), promoter-trapped transcripts (Tp-LacZ, 500 bp) and poly(A)-trapped transcripts (Tp-GFP, 308 bp), respectively. The PCR conditions were 98°C for 10 s, 68°C for 1 min, for 30 cycles. Primers for *ACTB*[18] were used as an internal control. PCR for *ACTB* was cycled 20 times at 94°C for 20 s, 60°C for 20 s, and 72°C for 30 s in a total volume of 10 μl containing 0.5 μl cDNA, 0.4 μM each primer, 0.2 mM each dNTP, 1 × ExTaq buffer, and 0.5 U ExTaq HS (Takara). All PCR products were electrophoresed on 2% agarose gels.

### In Situ Hybridization

Embryos were collected between E9.5 and E13.5. Whole-mount in situ hybridization was carried out as previously described.[19,20] Two fragments of *Smoc1* cDNA were obtained as probes by RT-PCR, with the use of total RNA extracted from livers of E16.5 mouse embryos, and subcloned into pCR4-TOPO (Invitrogen). Primer sequences were as follows: probe 1-F, 5′-GTCTGCTCACGCCCCACT-3′; probe 1-R, 5′-CCTGAACCATGTCTGTGGTG-3′; probe P-F, 5′-CAGGAACAGGAAAGGGAAGA-3′; probe P-R, 5′-AAGGGAAAACCACACAGCAC-3′. PCR products were 1023 bp and 1578 bp, corresponding to nucleotide positions 275–1297 and 1849–3426 of the mouse *Smoc1* cDNA (GenBank accession number NM_001146217.1), respectively. The cDNA fragment amplified with probe P-F and probe P-R primers was identical to the probe used in a previous report.[21] Digoxigenin-labeled sense and antisense riboprobes were synthesized with the use of a digoxigenin RNA labeling kit (Roche). These two different antisense probes demonstrated identical staining patterns, and the control sense probes showed no staining. The expression pattern was confirmed with more than three embryos. In addition, the following probes were used: *Bmp2* (gift from Y. Takahashi),[22] *Sox9* (gift from A. Yamada),[22] *Bmp7* (gift from E.J. Robertson), and *Msx2* (gift from Dr. R.E. Maxson, Jr). The numbers of embryos examined were as follows (numerical quantity for WT, *Smoc1*$^{Tp/+}$, and *Smoc1*$^{Tp/Tp}$, respectively, shown in parentheses): *Msx2* (2, 1, 3) at E11.5; *Bmp2* (3, 0, 3), *Bmp7* (3, 0, 3), *Msx2* (3, 0, 3), and *Sox9* (2, 1, 3) at E12.5; *Bmp2* (1, 2, 3), *Bmp7* (2, 1, 3), *Msx2* (1, 2, 3), and *Sox9* (1, 3, 4) at E13.5. Stained embryos were cleared in glycerol to enable images to be produced with a VHX-1000 digital microscope (Keyence).

### Histology

Heads of embryos and newborns were fixed overnight in 4% paraformaldehyde in PBS at 4°C. These embryos were then washed in PBS. Frozen samples were serially sectioned at 16 μm (E14.5) and 20 μm (P0). The numbers of eyes examined (WT, *Smoc1*$^{Tp/+}$, *Smoc1*$^{Tp/Tp}$) were as follows: coronally sectioned at E14.5 (8, 10, 12), coronally sectioned at P0 (8, 10, 6), horizontally sectioned at P0 (2, 2, 4). For evaluation of ventral atrophy of the retina, only the coronally sectioned eyes were used. TB staining was performed according to standard protocols. Forelimbs of mice were fixed in 4% paraformaldehyde in PBS, decalcified in 10% EDTA, and embedded in paraffin. Forelimbs were serially sectioned at 4 μm and stained with hematoxylin and eosin.

### Evaluation of Optic Nerve Diameter

The palatine and orbital bones were carefully removed to expose the optic chiasm and optic nerve. During the dissection process, 4% paraformaldehyde in PBS was frequently applied onto the gaps between the bone and optic nerve. Xylene cyanol was applied to enhance the outline of optic nerves at poastnatal day 0 (P0). Photographs of optic nerves were taken with a VHX-1000 digital microscope, and the diameter was measured for right and left optic nerves with the bundled software included with the VHX-1000 instrument.

### Skeletal Staining

For skeletal preparations, mice were fixed in 99.5% ethanol after removal of the skin and viscera. Cartilage tissues were stained with 0.015% alcian blue and 20% acetic acid in 75% ethanol for three days at 37°C. After dehydration with 99.5% ethanol for three days, bones were stained with 0.002% alizarin red in 1% KOH. Then skeletons were cleared in 1% KOH for several weeks. For P14 mice, soft tissues were dissolved in 2% KOH before alizarin red staining.

### Nile Blue Staining

For the study of apoptosis of hindlimbs at E13.5 and E14.5, Nile blue (NB) staining was performed on the basis of a previously described protocol,[23] except that staining was performed at 37°C (not room temperature). Apoptosis was determined by NB-stained (deceased) cells. After rinsing in Tyrode solution, hindlimbs of control (WT and heterozygous littermates) and homozygous mice were evaluated. Photographs of dorsal aspects were taken with a VHX-1000 digital microscope. Experiments were repeated three times, and reproducible representative results are presented.

### Statistical Analysis

Statistical analyses were performed with the use of non-repeated-measures ANOVA followed by Dunnett's post hoc test. The results are given as mean ± standard deviation, and the threshold p value for statistical significance was 0.01.

## Results

### Identification of Homozygous *SMOC1* Mutations

We have previously mapped the MLA locus to a 422 kb region at 10p11.23 by analyzing three families (one Japanese family [A] and two Lebanese families [B and C]). This region contained only one gene, *MPP7*, in which no mutations were found.[12] After a new Turkish family (X) was added to the analysis, the MLA locus was again searched by homozygosity mapping to the consanguineous families (X, B, and C) and haplotype mapping to family A for detection of compound-heterozygous mutations; however, we could not detect any common regions

among the four families. We then focused on identifying common regions in any three of the four families to allow for locus heterogeneity (Table S3).

A locus at 14q24.1-q24.2, which showed the highest LOD score (3.936) among the candidate regions larger than 2.0 Mb, was highlighted among families A, C, and X. This locus was analyzed with the use of additional microsatellite markers, and a 3.0 Mb region containing 24 genes was identified (Figures 1A and 1B). A total of 14 genes were sequenced, and homozygous mutations were found in *SMOC1*: c.718C>T (p.Gln240X) in family A, c.664+1G>A in family C, and c.378+1G>A in family X (Figures 1C and 1D). All of these homozygous mutations were cosegregated with the disease phenotype, and the parents of the individuals with these mutations were heterozygous carriers (Figure 1C). We could not find any mutations in *SMOC1* in family B, in which MLA is unlinked to the 14q24.1-q24.2 locus. Interestingly, in family A haplotypes of paternal and maternal alleles, each having the same mutation, are completely different (data not shown), suggesting that the same mutation may have occurred in separate events. The c.718C>T mutation was not detected in 289 healthy Japanese controls, including 100 Okinawa islanders. The other two mutations were not detected in ethnically matched controls (54 Lebanese and 99 Turkish subjects, respectively), nor in 289 Japanese controls. The two splice-donor-site mutations (c.664+1G>A and c.378+1G>A) are predicted to abolish a donor site, as predicted by ESEfinder, NetGene2, HSF2.4.1, SpliceView, and BDGP analysis (Table S4). Thus, the three mutations are likely to lead to a loss of functional SMOC1.

### *Smoc1* Expression in the Developing Eye and Limb in Mice

For the examination of *Smoc1* expression in the developing eye and limb, whole-mount in situ hybridization of mouse embryos was performed. *Smoc1* was expressed in the forebrain, midbrain, hindbrain, pharyngeal arch, somites, and forelimb buds at E9.5 (Figure 2A). At E10.5, *Smoc1* expression was observed in the optic stalk (Figure 2B), and at E11.5, expression was localized to the closure site of the optic cup (Figure 2C). Expression of *Smoc1* in developing limbs between E10.5 and E11.5 was observed in both dorsal and ventral regions, with a broader pattern of expression in dorsal regions, but expression was not detected in the most anterior, posterior, and distal parts of limb buds (Figures 2D and 2E). Expression coinciding with chondrogenic condensation was observed at E12.5 (Figure 2F), and expression then became restricted to future synovial joint regions at E13.5 (Figure 2G). This dynamic expression suggests that *Smoc1* plays a critical role in ocular and limb development.

### Ocular and Limb Anomalies in *Smoc1* Null Mice

To investigate the pathological basis of MLA due to the loss of *SMOC1* function, we obtained *Smoc1* mutant mice, PV384.[17] PV384 mice possess gene-trap insertions in the *Smoc1* locus and in three other loci. After PV384 mice were bred with C57BL/6J or ICR mice, we obtained three independent lines (no. 1 to no. 3), each with a sole insertion in intron 1 of *Smoc1* (Figure S1). We mainly analyzed line 1, but we confirmed similar phenotypes in lines 2 and 3. Heterozygous mutant mice ($Smoc1^{Tp/+}$) were healthy and fertile. Homozygous mice ($Smoc1^{TP/TP}$) were null mutants, as they showed no native transcript of *Smoc1* (Figure S1E). Homozygous mice were viable at P0; however, they did not survive beyond the first 3 wks of life (Figure 3B). Their growth was retarded in comparison to WT and heterozygous littermates at P0 and P14 (Figures 3A and 3C). Developmental defects in eyes and optic nerves were evident at E14.5. Homozygous mice had relatively small eyes, and histological examinations revealed aplasia or hypoplasia of optic nerves (in 10 of 12 optic nerves), atrophy of the anteroventral part of the retina (in 11 of 12 eyes), and extension of the retinal pigmented epithelium (RPE) to the optic nerve (in 10 of 12 eyes) (Figures 3D–3I). These abnormalities were also observed at P0 (aplasia or hypoplasia of optic nerves [in 7 of 10 optic nerves], retinal atrophy [in 6 of 6 eyes], and RPE extension [in 3 of 6 eyes with identifiable optic nerves]) (Figures 3J–3M). WT or heterozygous littermates did not show any such abnormalities, except that a few eyes of heterozygous mice showed extension of the RPE at E14.5, but not at P0 (in 2 of 10 and 0 of 12 eyes, respectively). Toluidine blue (TB) staining showed ganglion cell layers that were thinned and irregular to varying degrees in homozygous mice, suggesting a reduced number of retinal ganglion cells (Figures 3J–3K′). Thus, *Smoc1* is required for axon sprouting, elongation, or maintenance of retinal ganglion cells.[24] Hypoplasia of optic nerves was further quantitatively confirmed by macroscopic examination: the average diameter of optic nerves of homozygous mice was significantly smaller than that of WT and heterozygous littermates at P0 and P14 (Figures 3L–3Q). These data clearly demonstrate that loss of *Smoc1* in mice affects development of the body, retina, and optic nerves, in a manner similar to that seen in MLA patients.[3,4]

Newborn homozygous mice could be readily identified by their hindlimb syndactyly and pes valgus, whereas no abnormalities were observed in WT and heterozygous pups (Figure 4 and Table 1). Interestingly, the severity of syndactyly varied between mouse lines: line 1 exclusively showed soft tissue syndactyly, whereas line 2 frequently showed four digits (Figures 4F and 4J). Skeletal preparations with alcian blue and alizarin red revealed that the foot with four digits had four phalanx and five metatarsals with fusion to each other (Figure 4K). Thus the *Smoc1* null mutation resulted in a spectrum of phenotypes, from soft tissue syndactyly to four fused digits, probably due to different genetic backgrounds. Bowed tibiae and hypoplastic fibulae were also consistently observed in homozygous mice (Figures 4H and 4L). The articulation between

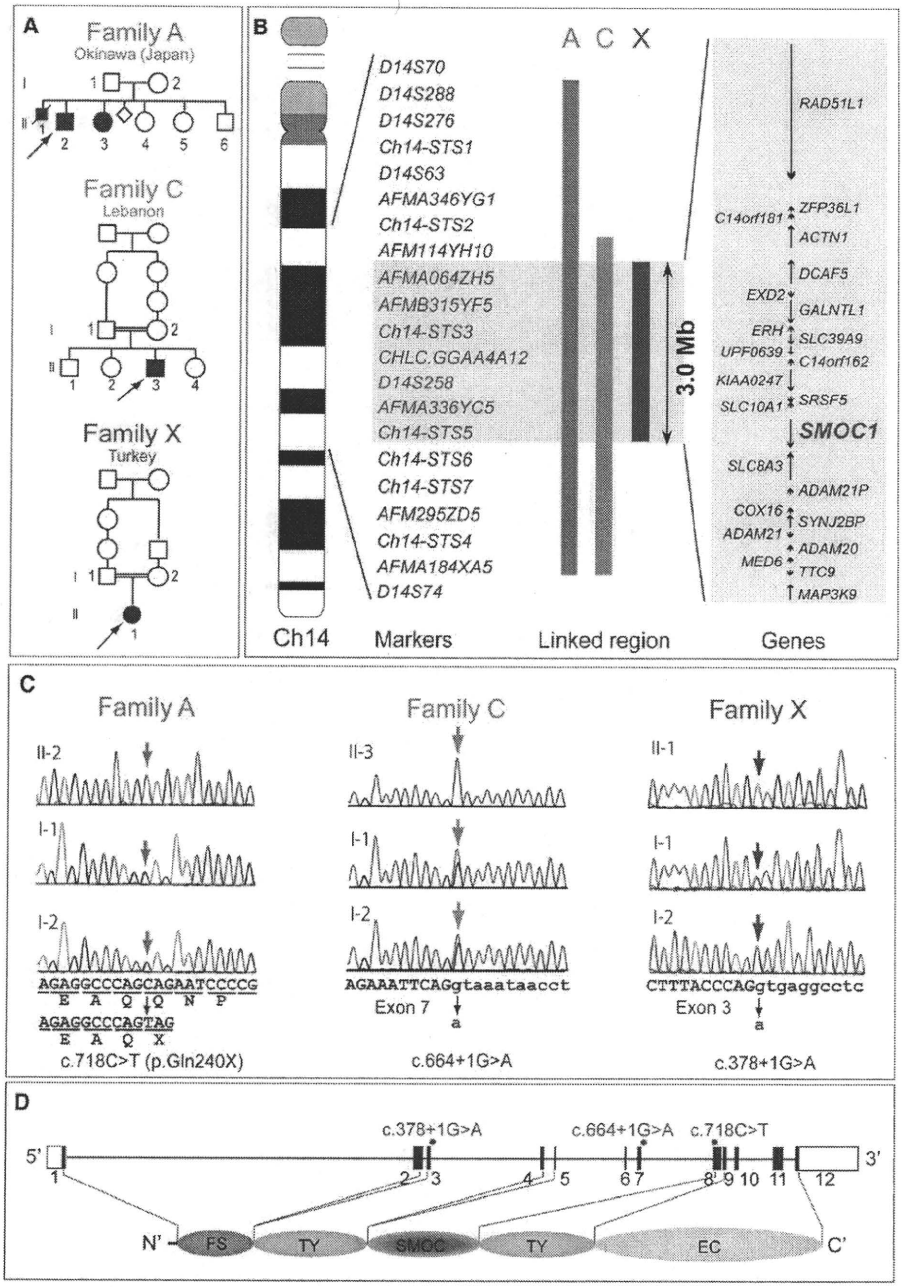


**Figure 1. Genetic Analysis of Three Families with Members Affected by Microphthalmia with Limb Anomalies**

(A) Pedigrees of the three families.

(B) Linkage analysis with SNPs and microsatellite markers on chromosome 14. From left to right: chromosome ideogram, genetic markers, linked regions of the three families, and genes mapped to the shortest overlapping linked region (between *AFM114YH10* and *Ch14-STS6* [UCSC coordinates, Feb. 2009: chromosome 14: 68,388,190–71,347,908 bp]).

(C) Sequences of mutations identified in each family. Affected patients in family A have a homozygous nonsense mutation (c.718C>T). Patients in families C and X have distinct homozygous splice-donor site mutations (c.664+1G>A and c.378+1G>A, respectively). For all mutations, parents of affected patients are heterozygous carriers, without exception. Sequences of the exon and intron are presented in upper and lower cases, respectively.

(D) At the top is a depiction of a schematic representation of *SMOC1* consisting of 12 exons (UTR and coding exons are indicated by open and filled rectangles, respectively). The locations of three mutations are indicated by red dots. At the bottom, the functional domains of SMOC1 are depicted. Abbreviations are as follows: FS, the follistatin-like domain; TY, the thyroglobulin-like domain; SMOC, the domain unique to SMOC; and EC, the extracellular calcium-binding domain.

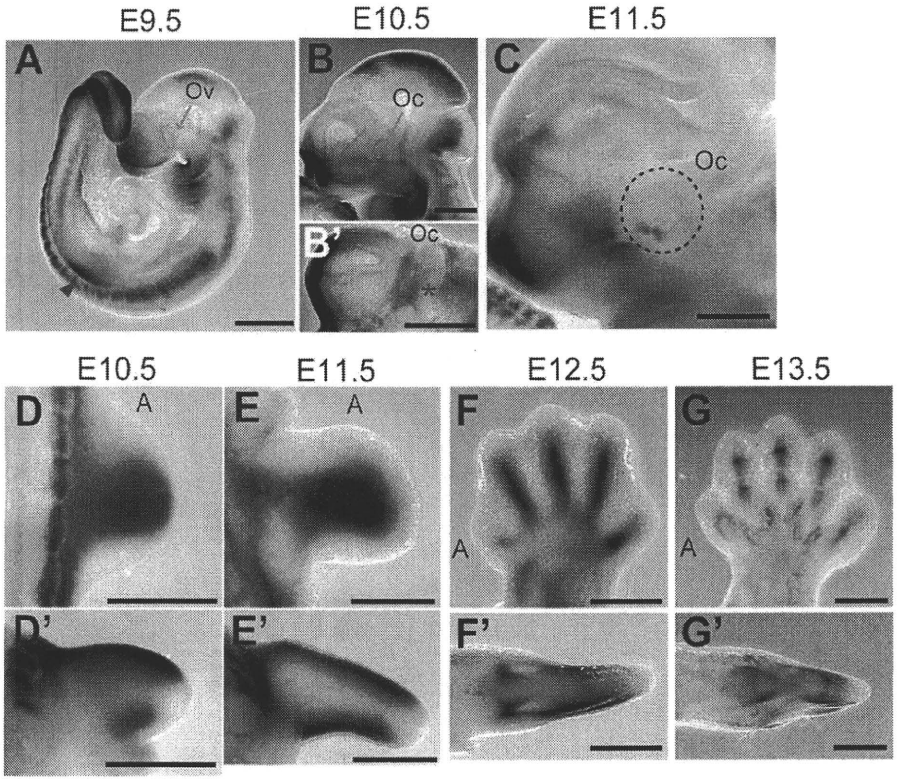


**Figure 2. *Smoc1* Expression in Mouse Embryos**
Lateral views of embryos (A–C) and a ventral view of the left part of the head (B′, lateral view is shown at the top).
(A) At E9.5, *Smoc1* was expressed in the forebrain, midbrain, hindbrain, pharyngeal arch, somites, and forelimb buds (magenta arrowhead), but not in the optic vesicle (Ov, blue arrow).
(B and B′) Expression in the optic stalk became evident at E10.5 (magenta asterisks), but was not evident in the optic cup (Oc, blue arrow).
(C) Expression was restricted to the closure site of the optic cup (dashed circle) at E11.5.
(D–G) Dorsal and (D′–G′) posterior view of the right hindlimbs (dorsal view is shown at the top in D′–G′). The anterior side is indicated by an A. (D and D′) At E10.5, *Smoc1* was more widely expressed in the dorsal part of the limb bud than in the ventral part. *Smoc1* expression is undetected in the most anterior, posterior, and distal parts of the limb bud. (E and E′) At E11.5, ventral expression was broader than that in the previous stage. (F and F′) At E12.5, expression was detected in areas consistent with chondrogenic condensation. (G and G′) At E13.5, *Smoc1* expression became restricted to future joint regions. Scale bar represents 500 μm.

tibia/fibula and calcanea of homozygous mice appeared malpositioned (Figures 4G and 4K), which might contribute to pes valgus. At P14, soft tissue syndactyly was also evident in most forelimbs of homozygous mice (Figures 4M–4O). Moreover, hindlimbs of homozygous mice showed synostosis between the $4^{th}$ and $5^{th}$ metatarsals (Figure 4T), which is observed in both the hands and the feet of MLA patients. Thus, many limb anomalies of MLA patients were recapitulated in *Smoc1* null mice (Table S1).

### Reduced Interdigital Apoptosis and Disturbed BMP Signaling

Among the various abnormalities caused by loss of *Smoc1* function, we focused on soft tissue syndactyly, which was commonly observed in both fore- and hindlimbs of null mutants. It is possible that the syndactyly is caused by failed apoptotic regression of the interdigital mesenchyme. To examine this hypothesis, hindlimbs were stained with NB sulfate at E13.5 and E14.5, the time when interdigital apoptosis is most evident. In control embryos (WT and heterozygous littermates), NB-stained apoptotic cells were identified in the interdigital mesenchyme, where regression of the interdigital webbing occurs in the distal region (Figures 5A and 5C). By contrast, the number of apoptotic cells in the mesenchyme between digits 2 and 3 and digits 3 and 4 was dramatically reduced in homozygous mice at E13.5 and E14.5, along with persistent webbing in the distal region (Figures 5B and 5D, magenta asterisk). BMP signaling is involved in apoptosis of the interdigital mesenchyme.[25,26] *Bmp2*, *Bmp7*, and *Msx2*, a direct target of BMP signaling, were strongly expressed in the interdigital mesenchyme of control hindlimbs at both E12.5 and E13.5. However, the expression of these three genes was profoundly reduced and perturbed in hindlimbs of homozygous mice (Figures 5E–5J). These data suggest that inhibition of apoptosis is spatiotemporally correlated to reduced and/or disturbed expression of genes involved in BMP signaling in the interdigital mesenchyme.

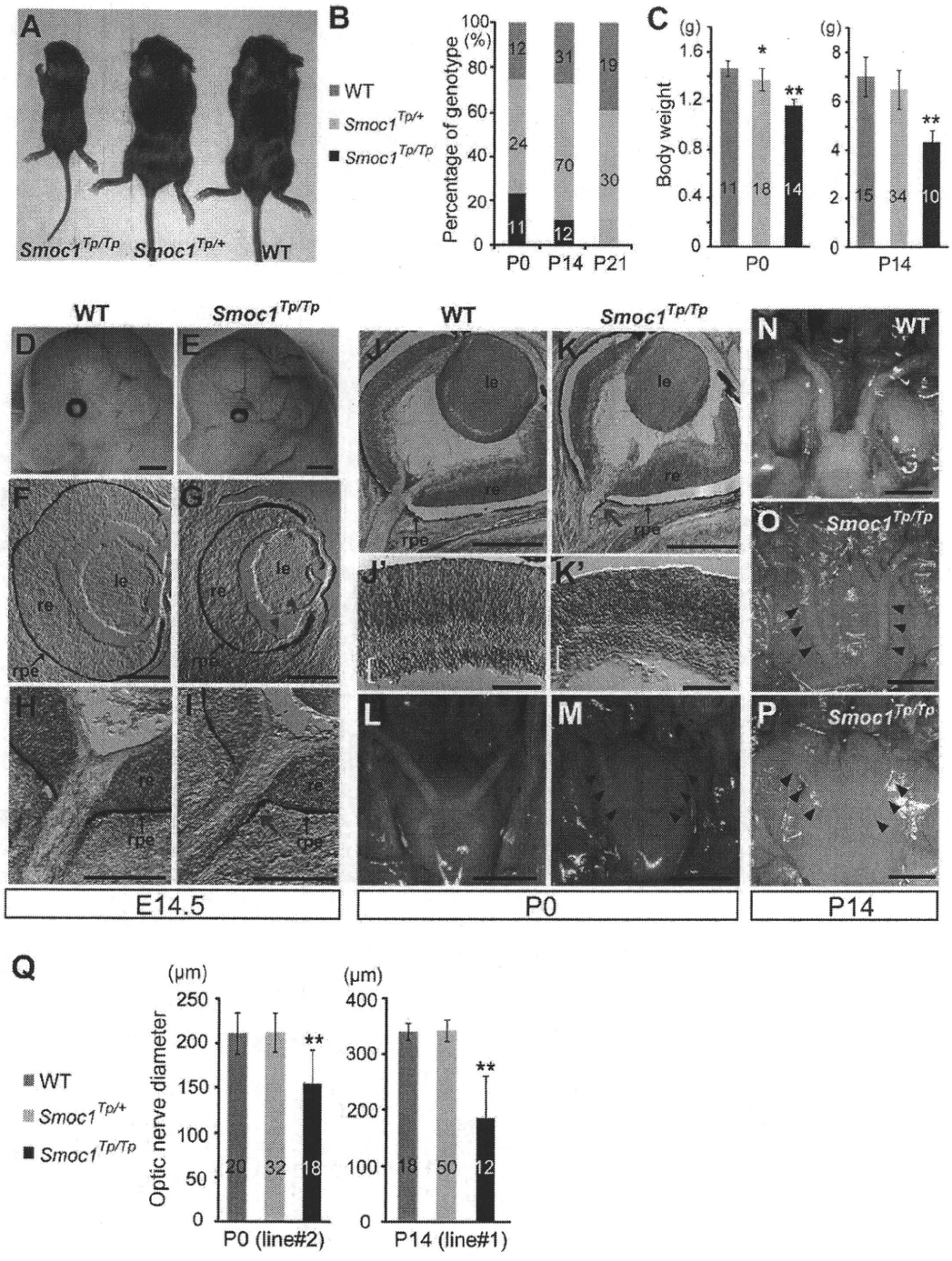


**Figure 3. Growth and Ocular Phenotypes of *Smoc1* Null Mice**

(A) Representative *Smoc1*$^{Tp/Tp}$ mouse, showing a small body in comparison to *Smoc1*$^{Tp/+}$ and WT littermates.

(B) Genotypes of living pups during the first 3 wk of life.

(C) Body weight of pups of each genotype at P0 (left panel) and P14 (right panel).

(D and E) Relatively small eyes were evident in *Smoc1*$^{Tp/Tp}$ mice in comparison to WT mice.

(F–K′) Coronal sections of eyes at E14.5 (F–I) and P0 (J–K′) with TB staining (H, I, and J–K′). (F-I) Atrophy of the anteroventral part of the retina (G, magenta arrowheads, dorsal view shown at the top), hypoplastic optic nerve, and extension of the RPE to the optic nerve (I, magenta arrow) in *Smoc1*$^{Tp/Tp}$ mice at E14.5. (J and K) Hypoplastic optic nerve and RPE extension in *Smoc1*$^{Tp/Tp}$ mice at P0 (K, magenta arrow). Note that sections in which optic nerves appeared most thick are presented in (H–K). (J′–K′) In higher-magnification views of (J and K), a thinned and irregular ganglion cell layer (white brackets) was observed in *Smoc1*$^{Tp/Tp}$ mice. Abbreviations are as follows: le, lens; re, retina; rpe, retinal pigmented epithelium.

(L–P) Ventral views of the brain showing optic nerves at P0 (L and M) and P14 (N–P), showing various degrees of optic nerve hypoplasia.

## Discussion

In a previous report, we performed parametric linkage analysis with three families (families A, B, and C) and found 16 loci showing a LOD score ($\theta = 0.000$) higher than 3.0. Additional microsatellite markers highlighted only one locus, 10p11.23.[12] However, no mutations were found in the candidate gene *MPP7*.[12] By recruiting a new family (family X) to this study, we successfully found homozygous mutations in *SMOC1* in families A, C, and X. In family B, no *SMOC1* mutations were found, indicating the genetic heterogeneity in MLA. Patients with *SMOC1* mutations and *Smoc1* null mice showed similar limb anomalies, such as oligodactyly, syndactyly, synostosis of 4th and 5th metacarpals, hypoplasia of fibula, and bowed tibia. Oligodactyly, syndactyly, and synostosis of 4th and 5th metacarpals are common in MLA patients.[2–4] However, hypoplastic fibula and bowed tibia are less common in patients with MLA, as four out of 34 MLA patients showed these anomalies in the previous report.[3] Although one patient with a *SMOC1* mutation from family C did not show bowed tibia and hypoplastic fibula, these anomalies could be features specific to *SMOC1* mutations. Further *SMOC1* analysis of other MLA patients should delineate the phenotypic consequences caused by *SMOC1* mutations.

Accumulating evidence suggests that BMP signaling plays crucial roles in early eye vesicle and limb patterning, skeletal formation, and apoptosis of the interdigital mesenchyme,[25–29] and mutations involving BMP signaling cause human malformations including ocular, limb, and skeletal anomalies.[7,30–33] Here, we present genetic evidence that *SMOC1* is essential for ocular and limb development in humans and mice. Furthermore, *Xenopus smoc* can inhibit BMP signaling,[11] suggesting that *SMOC1/Smoc1* can also modulate BMP signaling in humans and mice. Indeed, we observed reduced and/or disturbed expression of genes involved in BMP signaling in the interdigital mesenchyme in *Smoc1* null mice, and limb and ocular abnormalities associated with loss of *Smoc1* function are consistent with phenotypic consequences of disturbed BMP signaling. Conditional inactivation of *Bmp2* in the limb showed 3/4 syndactyly, and a similar deficiency of both *Bmp2* and *Bmp7* resulted in malformed fibulae in mice.[25] Moreover, mice deficient in *Fmn1*, a repressor of BMP signaling, showed four digits, fused metatarsal bones, and an absence of fibulae in the hindlimbs,[34] suggesting the importance of altered BMP signaling in these features. Concerning ocular phenotypes, haploinsufficiency of mouse *Bmp4* resulted in a decreased number of ganglion layer cells and absence of the optic nerve similar to *Smoc1* null mice,[35] indicating that altered BMP signaling is also involved in the ocular phenotype. Interestingly, knockdown experiments of *smoc* by antisense morpholino in *Xenopus* showed absence or severe deformity of the eye and other anterior structures, which were accompanied by aberrant expression of *otx2*, *tbx2* in the eye field.[11] Mutations of *OTX2* (MIM 600037) cause micropthalmia, syndromic 5 (MCOPS5 [MIM 610125]) in humans.[36] Moreover, targeted disruption of *Tbx2* resulted in a marked reduction in the size of the optic cup and a failure of optic nerve formation in mice.[37] Thus, it is possible that loss of *SMOC1* function could alter the expression of *OTX2* and *TBX2* (MIM 600747) by disturbing BMP signaling in human developing eyes.

It is unknown how the loss of functional SMOC1, a BMP antagonist, leads to reduced expression of genes involved in BMP signaling in the interdigital mesenchyme in *Smoc1* null mice. In the case of *Fmn1*-deficient mice, the loss of the repressor of BMP signaling resulted in downregulation of *Fgf4* and *Shh* and in upregulation of *Gremlin* expression at E10.5, and absence of apoptosis of the interdigital mesenchyme between the two middle digits at E13.5.[34] Thus, there is a possibility that loss of SMOC1 could cause the imbalance among BMP, SHH, and FGF signaling, which would subsequently lead to reduced and/or disturbed expression of genes involved in BMP signaling in the interdigital mesenchyme. In fact, we observed reduced expression of *Msx2* in the progressive zone of hindlimbs at E11.5 (Figure S2). Moreover, expression of *Sox9*, the initial cartilage condensation marker, showed abnormal limb patterning, suggesting that SMOC1 may affect BMP signaling even at early stages of limb development (Figure S3). Further examinations are required for understanding spatial and temporal actions of SMOC1/Smoc1 protein during limb development.

In conclusion, our data demonstrate that *SMOC1/Smoc1* is an essential player in both ocular and limb development in humans and mice and give further support to the crucial roles of BMP signaling in these systems.

### Supplemental Data

Supplemental Data include three figures and four tables and can be found with this article online at http://www.cell.com/AJHG/.

### Acknowledgments

We would like to thank the patients and their families for their participation in this study. We thank Yoshiko Takahashi (Nara Institute of Science and Technology) and Atsushi Yamada (Showa University) for providing the *Bmp2* and *Sox9* probes; Elizabeth J. Robertson (University of Oxford) and Makoto Ishibashi (Kyoto University) for the *Bmp7* probe; Robert E. Maxson, Jr. (University of Southern California Keck School of Medicine) for the *Msx2*

(Q) Optic nerve diameter. Optic nerves were significantly hypoplastic in $Smoc1^{Tp/Tp}$ mice in comparison to WT and $Smoc1^{Tp/+}$ littermates. The numbers of pups (B and C) or eyes (Q) corresponding to each genotype are indicated within bars. Error bars indicate standard deviation: *$p < 0.01$, compared with WT. **$p < 0.01$, compared with WT and $Smoc1^{Tp/+}$. Scale bars represent 1 mm (D, E, and L–P), 200 μm (F–I), 500 μm (J and K), and 100 μm (J′ and K′).

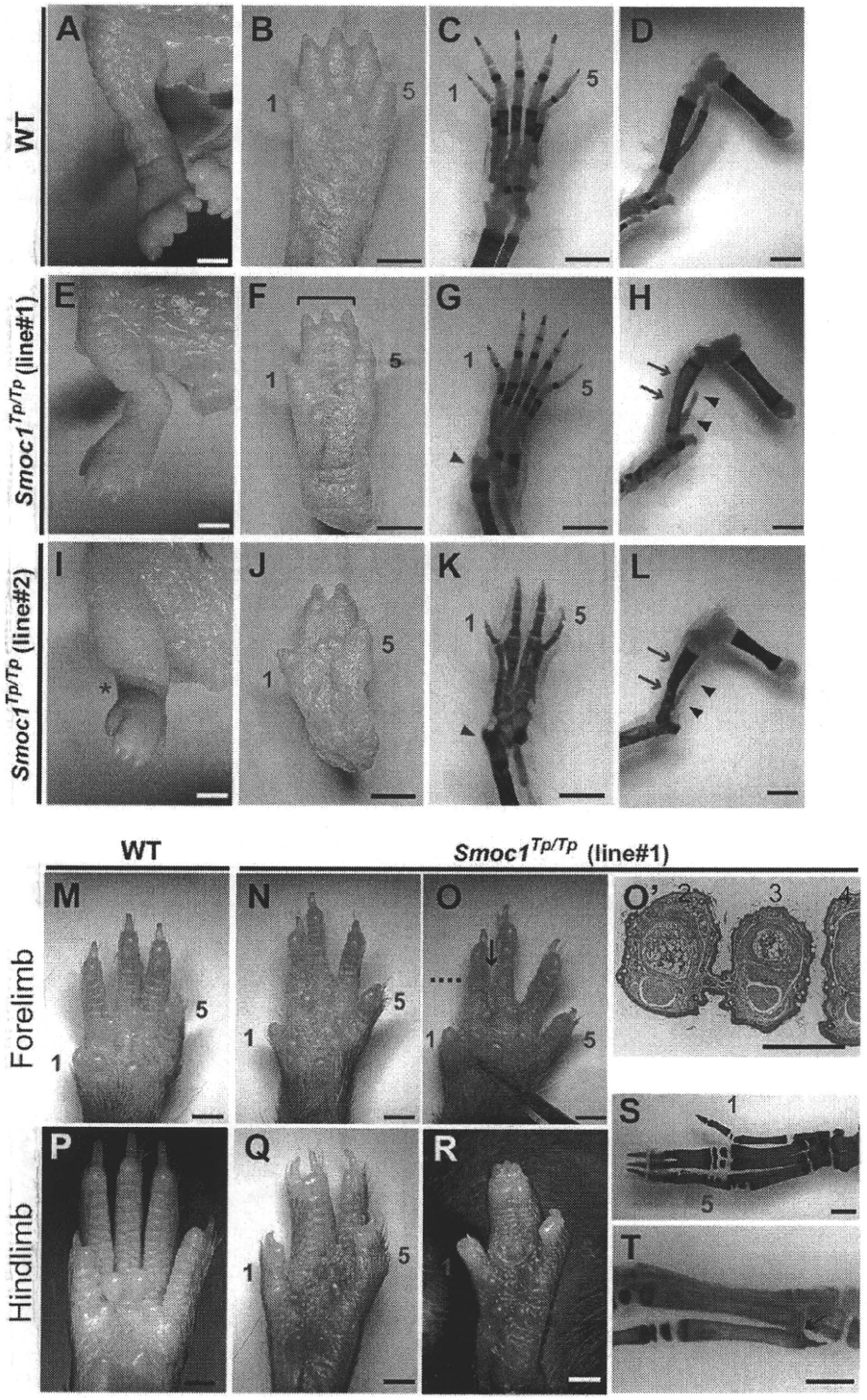


**Figure 4. Limb Phenotypes of *Smoc1* Null Mice**

Limbs of WT (A–D, M, and P) and *Smoc1*$^{Tp/Tp}$ mice (E–L, N–O′, and Q–T) at P0 (A–L) and P14 (M–T). Digit identities are indicated by the numbers 1 (thumb, anterior) and 5 (little finger, posterior). Skeletal staining with alcian blue and alizarin red is presented (C, D, G, H, K, L, S, and T). *Smoc1*$^{Tp/Tp}$ mice showed pes valgus (E and I), soft tissue syndactyly (F and G), and four digits with metatarsal fusion (J and K). Malposition of the articulation between the tibia/fibula and the calcanea (G and K, magenta arrowheads), bowed tibia (magenta arrows), and hypoplastic fibula (arrowheads) of *Smoc1*$^{Tp/Tp}$ mice (H and L) were observed. 2/3 soft tissue syndactyly (N) and 2/3 webbing (O) were evident in forelimbs of *Smoc1*$^{Tp/Tp}$ mice. (O′) A transverse section taken at the level indicated by the dashed line in (O) showed 2/3 webbing. 2/3 syndactyly (Q), 2/3/4 syndactyly (R), synostosis between the 2$^{nd}$ and 3$^{rd}$ proximal phalanx and metatarsals (S), and synostosis between the 4$^{th}$ and 5$^{th}$ metatarsals (T, arrow), observed in the hindlimbs of *Smoc1*$^{Tp/Tp}$ mice. Scale bars represent 1 mm (A–O and P–T) or 500 μm (O′).

**Table 1. Limb Abnormalities in *Smoc1*$^{Tp/Tp}$ Mutants**

| Genotype | Talipes Valgus (No. of Affected/ Total No. of Pups) | Forelimb Abnormalities (No. of Limbs) | Hindlimb Syndactyly (No. of Limbs) | | | | | Other External Abnormalities (No. of Pups) | 4th and 5th Metatarsal Fusion (No. of Affected/Total No. of Limbs) |
|---|---|---|---|---|---|---|---|---|---|
| | | | None | 2/3[a] | 3/4[b] | 2/3/4[c] | 4 Digits | | |
| **Postnatal Day 0** | | | | | | | | | |
| *Smoc1*$^{Tp/+}$ (line 1, C57BL/6J) | 0/42 | 0 | 84 | 0 | 0 | 0 | 0 | | |
| *Smoc1*$^{Tp/+}$ (line 2, ICR mixed) | 0/38 | 0 | 76 | 0 | 0 | 0 | 0 | | |
| *Smoc1*$^{Tp/Tp}$ (line 1, C57BL/6J) | 10/10 | 0 | 3 | 0 | 3 | 12 | 2 | | |
| *Smoc1*$^{Tp/Tp}$ (line 2, ICR mixed) | 13/17 | 1[d] | 1 | 1 | 9 | 4 | 19 | cleft palate (3) | |
| **Postnatal Day 14** | | | | | | | | | |
| *Smoc1*$^{Tp/+}$ (line 1, C57BL/6J) | 0/70 | 0 | 140 | 0 | 0 | 0 | 0 | | |
| *Smoc1*$^{Tp/Tp}$ (line 1, C57BL/6J) | 11/11 | 18[e] | 2 | 7 | 3 | 8 | 2 | hypoplastic thumbs (5) | 9/10[f] |

[a] Syndactyly between the 2nd and 3rd digits.
[b] Syndactyly between the 3rd and 4th digits.
[c] Syndactyly between the 2nd, 3rd, and 4th digits.
[d] 2/3 soft tissue syndactyly.
[e] Eleven limbs showed 2/3 webbing, four limbs showed 2/3 soft tissue syndactyly, and one limb showed 3/4 syndactyly.
[f] Based on examination of skeletal preparations.

probe; Tomonori Hirose, Kazunori Akimoto, and Kazunori Sasaki (Yokohama City University) for providing useful information about mouse breeding, taking photos on a stereo microscope, and mRNA quantification; and Kohei Shiota and Sumiko Kimura (Kyoto University) for helpful comments about NB staining and limb anomalies. This work was supported by research grants from the Ministry of Health, Labour and Welfare (T. Furuichi, N. Miyake, N. Matsumoto, and H.S.) and the Japan Science and Technology Agency (N. Matsumoto), a Grant-in-Aid for Scientific Research from the Japan Society for the Promotion of Science (T. Furuichi and N. Matsumoto), and a Grant-in-Aid for Young Scientist from the Japan Society for the Promotion of Science (K.N., H.D., N. Miyake, and H.S.). This work has been carried out at the Advanced Medical Research Center of Yokohama City University.

Received: September 29, 2010
Revised: November 20, 2010
Accepted: November 26, 2010
Published online: December 30, 2010

## Web Resources

The URLs for data presented herein are as follows:

BDGP, http://www.fruitfly.org/
ESEfinder 3.0, http://rulai.cshl.edu/cgi-bin/tools/ESE3/esefinder.cgi?process=home
GenBank, http://www.ncbi.nlm.nih.gov/Genbank/
HSF2.4.1, http://www.umd.be/HSF/
NetGene2, http://www.cbs.dtu.dk/services/NetGene2/
Online Mendelian Inheritance in Man, http://www.ncbi.nlm.nih.gov/Omim
UCSC Genome Browser, http://genome.ucsc.edu/cgi-bin/hgGateway
SpliceView, http://zeus2.itb.cnr.it/~webgene/wwwspliceview.html

## References

1. Waardenburg, P.J. (1961). Autosomally-recessive anophthalmia with malformations of the hands and feet. In Genetics and Ophthalmology, P.J. Waardenburg, A. Franceschetti, and D. Klein, eds. (Assen, The Netherlands: Royal Van Gorcum), p. 773.
2. Teiber, M.L., Garrido, J.A., and Barreiro, C.Z. (2007). Ophthalmo-acromelic syndrome: report of a case with vertebral anomalies. Am. J. Med. Genet. A. *143A*, 2460–2462.
3. Garavelli, L., Pedori, S., Dal Zotto, R., Franchi, F., Marinelli, M., Croci, G.F., Bellato, S., Ammenti, A., Virdis, R., Banchini, G., and Superti-Furga, A. (2006). Anophthalmos with limb anomalies (Waardenburg opththalmo-acromelic syndrome): report of a new Italian case with renal anomaly and review. Genet. Couns. *17*, 449–455.
4. Tekin, M., Tutar, E., Arsan, S., Atay, G., and Bodurtha, J. (2000). Ophthalmo-acromelic syndrome: report and review. Am. J. Med. Genet. *90*, 150–154.
5. Adler, R., and Canto-Soler, M.V. (2007). Molecular mechanisms of optic vesicle development: complexities, ambiguities and controversies. Dev. Biol. *305*, 1–13.
6. Zeller, R., López-Ríos, J., and Zuniga, A. (2009). Vertebrate limb bud development: moving towards integrative analysis of organogenesis. Nat. Rev. Genet. *10*, 845–858.
7. Bakrania, P., Efthymiou, M., Klein, J.C., Salt, A., Bunyan, D.J., Wyatt, A., Ponting, C.P., Martin, A., Williams, S., Lindley, V., et al. (2008). Mutations in BMP4 cause eye, brain, and digit

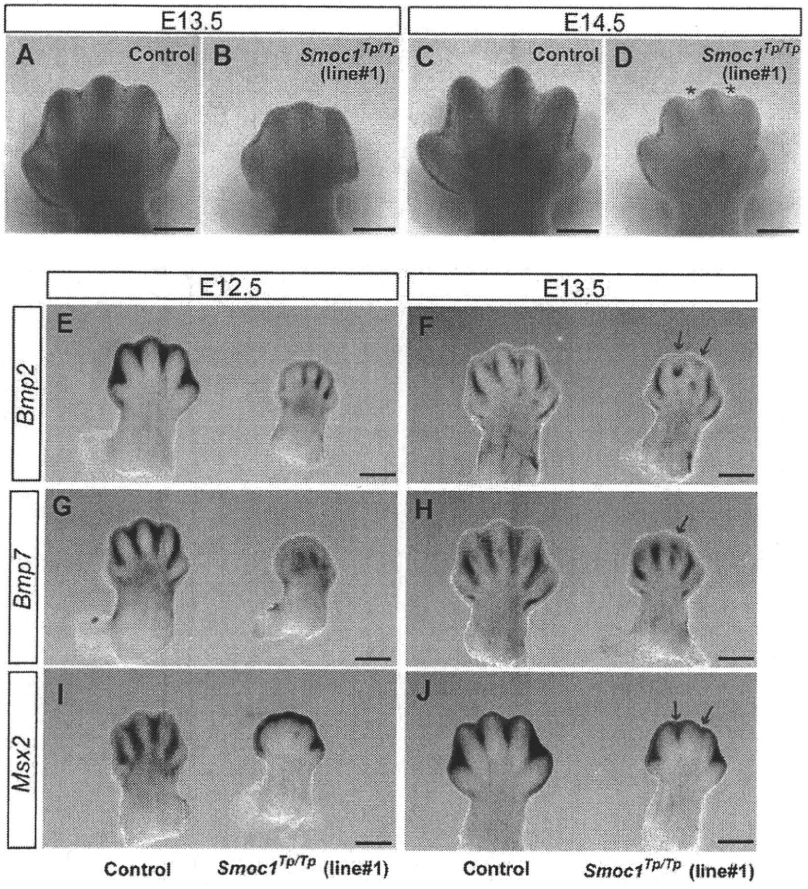


**Figure 5. Reduced Apoptosis and Altered BMP Signaling in the Interdigital Mesenchyme of *Smoc1* Null Mice**

(A–D) NB staining of left hindlimbs at E13.5 (A and B) and E14.5 (C and D). In comparison to control embryos (WT and $Smoc1^{Tp/+}$ littermates) (A and C), the number of NB-stained apoptotic cells in the interdigital mesenchyme of $Smoc1^{Tp/Tp}$ mice was dramatically reduced between digits 2 and 3 and digits 3 and 4 at both E13.5 and E14.5, and the webbing remained at a distal level (B and D, magenta asterisk).

(E–J) Whole-mount in situ hybridization of right hindlimbs at E12.5 (E, G, and I) and E13.5 (F, H, and J). At E12.5, interdigital expression of *Bmp2*, *Bmp7*, and *Msx2* was profoundly delayed in the hindlimbs of $Smoc1^{Tp/Tp}$ mice, and their expression in the interdigital mesenchyme was apparently perturbed, even at E13.5 (magenta arrows). Scale bar represents 500 μm.

developmental anomalies: overlap between the BMP4 and hedgehog signaling pathways. Am. J. Hum. Genet. *82*, 304–319.

8. Bornstein, P., and Sage, E.H. (2002). Matricellular proteins: extracellular modulators of cell function. Curr. Opin. Cell Biol. *14*, 608–616.
9. Vannahme, C., Smyth, N., Miosge, N., Gösling, S., Frie, C., Paulsson, M., Maurer, P., and Hartmann, U. (2002). Characterization of SMOC-1, a novel modular calcium-binding protein in basement membranes. J. Biol. Chem. *277*, 37977–37986.
10. Gersdorff, N., Müller, M., Schall, A., and Miosge, N. (2006). Secreted modular calcium-binding protein-1 localization during mouse embryogenesis. Histochem. Cell Biol. *126*, 705–712.
11. Thomas, J.T., Canelos, P., Luyten, F.P., and Moos, M., Jr. (2009). Xenopus SMOC-1 inhibits BMP signaling downstream of receptor binding and is essential for post-gastrulation development in Xenopus. J. Biol. Chem. *284*, 18994–19005.
12. Hamanoue, H., Megarbane, A., Tohma, T., Nishimura, A., Mizuguchi, T., Saitsu, H., Sakai, H., Miura, S., Toda, T., Miyake, N., et al. (2009). A locus for ophthalmo-acromelic syndrome mapped to 10p11.23. Am. J. Med. Genet. A. *149A*, 336–342.
13. Mégarbané, A., Souraty, N., and Tamraz, J. (1998). Ophthalmo-acromelic syndrome (Waardenburg) with split hand and polydactyly. Genet. Couns. *9*, 195–199.
14. Cogulu, O., Ozkinay, F., Gündüz, C., Sapmaz, G., and Ozkinay, C. (2000). Waardenburg anophthalmia syndrome: report and review. Am. J. Med. Genet. *90*, 173–174.
15. Miyake, N., Kosho, T., Mizumoto, S., Furuichi, T., Hatamochi, A., Nagashima, Y., Arai, E., Takahashi, K., Kawamura, R., Wakui, K., et al. (2010). Loss-of-function mutations of CHST14 in a new type of Ehlers-Danlos syndrome. Hum. Mutat. *31*, 966–974.
16. Gudbjartsson, D.F., Thorvaldsson, T., Kong, A., Gunnarsson, G., and Ingolfsdottir, A. (2005). Allegro version 2. Nat. Genet. *37*, 1015–1016.
17. Keng, V.W., Yae, K., Hayakawa, T., Mizuno, S., Uno, Y., Yusa, K., Kokubu, C., Kinoshita, T., Akagi, K., Jenkins, N.A., et al. (2005). Region-specific saturation germline mutagenesis in mice using the Sleeping Beauty transposon system. Nat. Methods *2*, 763–769.
18. Mamo, S., Gal, A.B., Bodo, S., and Dinnyes, A. (2007). Quantitative evaluation and selection of reference genes in mouse oocytes and embryos cultured in vivo and in vitro. BMC Dev. Biol. *7*, 14.
19. Parr, B.A., Shea, M.J., Vassileva, G., and McMahon, A.P. (1993). Mouse Wnt genes exhibit discrete domains of expression in the early embryonic CNS and limb buds. Development *119*, 247–261.
20. Saitsu, H., Ishibashi, M., Nakano, H., and Shiota, K. (2003). Spatial and temporal expression of folate-binding protein 1 (Fbp1) is closely associated with anterior neural tube closure in mice. Dev. Dyn. *226*, 112–117.
21. Tamplin, O.J., Kinzel, D., Cox, B.J., Bell, C.E., Rossant, J., and Lickert, H. (2008). Microarray analysis of Foxa2 mutant mouse embryos reveals novel gene expression and inductive roles

for the gastrula organizer and its derivatives. BMC Genomics *9*, 511.

22. Suzuki, D., Yamada, A., Amano, T., Yasuhara, R., Kimura, A., Sakahara, M., Tsumaki, N., Takeda, S., Tamura, M., Nakamura, M., et al. (2009). Essential mesenchymal role of small GTPase Rac1 in interdigital programmed cell death during limb development. Dev. Biol. *335*, 396–406.
23. Kimura, S., and Shiota, K. (1996). Sequential changes of programmed cell death in developing fetal mouse limbs and its possible roles in limb morphogenesis. J. Morphol. *229*, 337–346.
24. Sernagor, E., Eglen, S.J., and Wong, R.O. (2001). Development of retinal ganglion cell structure and function. Prog. Retin. Eye Res. *20*, 139–174.
25. Bandyopadhyay, A., Tsuji, K., Cox, K., Harfe, B.D., Rosen, V., and Tabin, C.J. (2006). Genetic analysis of the roles of BMP2, BMP4, and BMP7 in limb patterning and skeletogenesis. PLoS Genet. *2*, e216.
26. Robert, B. (2007). Bone morphogenetic protein signaling in limb outgrowth and patterning. Dev. Growth Differ. *49*, 455–468.
27. Dudley, A.T., Lyons, K.M., and Robertson, E.J. (1995). A requirement for bone morphogenetic protein-7 during development of the mammalian kidney and eye. Genes Dev. *9*, 2795–2807.
28. Khokha, M.K., Hsu, D., Brunet, L.J., Dionne, M.S., and Harland, R.M. (2003). Gremlin is the BMP antagonist required for maintenance of Shh and Fgf signals during limb patterning. Nat. Genet. *34*, 303–307.
29. Furuta, Y., and Hogan, B.L. (1998). BMP4 is essential for lens induction in the mouse embryo. Genes Dev. *12*, 3764–3775.
30. Asai-Coakwell, M., French, C.R., Berry, K.M., Ye, M., Koss, R., Somerville, M., Mueller, R., van Heyningen, V., Waskiewicz, A.J., and Lehmann, O.J. (2007). GDF6, a novel locus for a spectrum of ocular developmental anomalies. Am. J. Hum. Genet. *80*, 306–315.
31. Tassabehji, M., Fang, Z.M., Hilton, E.N., McGaughran, J., Zhao, Z., de Bock, C.E., Howard, E., Malass, M., Donnai, D., Diwan, A., et al. (2008). Mutations in GDF6 are associated with vertebral segmentation defects in Klippel-Feil syndrome. Hum. Mutat. *29*, 1017–1027.
32. Wyatt, A.W., Osborne, R.J., Stewart, H., and Ragge, N.K. (2010). Bone morphogenetic protein 7 (BMP7) mutations are associated with variable ocular, brain, ear, palate, and skeletal anomalies. Hum. Mutat. *31*, 781–787.
33. Ye, M., Berry-Wynne, K.M., Asai-Coakwell, M., Sundaresan, P., Footz, T., French, C.R., Abitbol, M., Fleisch, V.C., Corbett, N., Allison, W.T., et al. (2010). Mutation of the bone morphogenetic protein GDF3 causes ocular and skeletal anomalies. Hum. Mol. Genet. *19*, 287–298.
34. Zhou, F., Leder, P., Zuniga, A., and Dettenhofer, M. (2009). Formin1 disruption confers oligodactylism and alters Bmp signaling. Hum. Mol. Genet. *18*, 2472–2482.
35. Chang, B., Smith, R.S., Peters, M., Savinova, O.V., Hawes, N.L., Zabaleta, A., Nusinowitz, S., Martin, J.E., Davisson, M.L., Cepko, C.L., et al. (2001). Haploinsufficient Bmp4 ocular phenotypes include anterior segment dysgenesis with elevated intraocular pressure. BMC Genet. *2*, 18.
36. Ragge, N.K., Brown, A.G., Poloschek, C.M., Lorenz, B., Henderson, R.A., Clarke, M.P., Russell-Eggitt, I., Fielder, A., Gerrelli, D., Martinez-Barbera, J.P., et al. (2005). Heterozygous mutations of OTX2 cause severe ocular malformations. Am. J. Hum. Genet. *76*, 1008–1022.
37. Behesti, H., Papaioannou, V.E., and Sowden, J.C. (2009). Loss of Tbx2 delays optic vesicle invagination leading to small optic cups. Dev. Biol. *333*, 360–372.

CLINICAL GENETICS
An International Journal of Genetics, Molecular, and Personalized Medicine

*Clin Genet 2010*
*Printed in Singapore. All rights reserved*



CLINICAL GENETICS
doi: 10.1111/j.1399-0004.2010.01554.x

## Short Report

# Familial Simpson–Golabi–Behmel syndrome: studies of X-chromosome inactivation and clinical phenotypes in two female individuals with *GPC3* mutations

Yano S, Baskin B, Bagheri A, Watanabe Y, Moseley K, Nishimura A, Matsumoto N, Ray PN. Familial Simpson–Golabi–Behmel syndrome: studies of X-chromosome inactivation and clinical phenotypes in two female individuals with *GPC3* mutations.
Clin Genet 2010. © John Wiley & Sons A/S, 2010

Simpson–Golabi–Behmel syndrome (SGBS) is an overgrowth/multiple congenital anomalies syndrome with an X-linked inheritance. Most cases of SGBS are attributed to mutations in the glypican 3-gene (*GPC3*), which is highly expressed in the mesodermal embryonic tissues and involves in a local growth regulation. Typical clinical features include pre/postnatal overgrowth, developmental delay, macrocephaly, characteristic facies with prominent eyes and macroglossia, diaphragmatic hernia, congenital heart defects, kidney anomalies, and skeletal anomalies. Obligate carrier females with *GPC3* mutations are usually asymptomatic or with mild symptoms. It is thought that skewed X-inactivation is the underlining mechanism for the female patients to present with findings of SGBS. We identified three siblings with typical SGBS (two male and one female cases) and their mother with very mild symptoms in a family carrying c.256C>T (p.Arg86X) mutation in *GPC3*. X-inactivation studies on the androgen-receptor gene (*AR*) and the Fragile XE (FRAXE) gene were performed with blood, buccal swabs, and fibroblasts in the carrier females. The studies with blood showed moderately skewed X-inactivation with paternal X-chromosome being preferentially inactivated (71–80% inactivated) in the female patient with SGBS and no skewing was shown in the mother with very mild symptoms. The X-inactivation studies in the mother showed inactivation of the X-chromosome with the mutation by 57%. This suggests that loss of the functional GPC3 protein by 43% is closed to the threshold to develop the SGBS phenotype. Studies with buccal swabs and fibroblasts failed to show different X-inactivation patterns between the two female individuals.

### Conflict of interest

Nothing to declare.

**S Yano[a], B Baskin[b], A Bagheri[a], Y Watanabe[c], K Moseley[a], A Nishimura[d], N Matsumoto[d] and PN Ray[b]**

[a]Genetics Division, Department of Pediatrics, LAC+USC Medical Center, Keck School of Medicine, University of Southern California, Los Angeles, CA, USA, [b]Division of Molecular Genetics, Department of Pediatric Laboratory Medicine, The Hospital for Sick Children, Toronto, ON, Canada, [c]Department of Pediatrics and Child Health, Kurume University School of Medicine, Kurume, Japan, and [d]Department of Human Genetics, Yokohama City University Graduate School of Medicine, Yokohama, Japan

Key words: buccal swabs – GPC3 – skewed X-chromosome inactivation – SGBS – skin fibroblasts

Corresponding author: Shoji Yano, Genetics Division, Department of Pediatrics, LAC+USC Medical Center, Keck School of Medicine, University of Southern California, Los Angeles, CA, USA.
Tel.: +1-323-226-3816;
fax: +1-323-226-6073;
e-mail: syano@usc.edu

Received 24 July 2010, revised and accepted for publication 20 September 2010

## Introduction

Simpson–Golabi–Behmel syndrome (SGBS) is an X-linked overgrowth syndrome characterized by pre- and postnatal macrosomia, macrocephaly, characteristic facies including hypertelorism, macrostomia, macroglossia, mental retardation, and other variable anomalies including congenital diaphragmatic hernia, congenital heart defects, renal defects, gastrointestinal anomalies, and skeletal anomalies including vertebral fusion, scoliosis, pectus excavatum, and rib anomalies (1–5). An incidence of neoplasia is reported to be approximately 10% in patients with SGBS (6). The glypican 3 (*GPC3*) gene is the only gene known to cause SGBS, although a severe variant form has recently been mapped to Xp22 (7, 8). *GPC3* is located at Xq26 and encodes the glypican-3 protein which is a glycosylphosphatidylinositol-linked cell surface heparan sulfate proteoglycan. It is thought to play an important role in growth control in embryonic mesoderm derived tissues (7). SGBS has a wide range of clinical manifestations and genotype–phenotype correlations have not been recognized (7, 9). Mutations in *GPC3* causing SGBS are believed to result in a loss-of-function of the glypican-3 protein (10). Although, carrier females can have mild manifestations of SGBS, they do not usually have typical clinical features of SGBS (2, 11). A female with typical SGBS with an X-autosome translocation has been reported (12). These observations likely suggest that skewed X-inactivation is the underlining mechanism for wide clinical phenotypic manifestations in female carriers with *GLP3* mutations.

## Aims of the study

The aim of the study was to evaluate if skewed X-chromosome inactivation was responsible for female patients with *GPC3* mutations to develop clinical features of SGBS.

## Subjects and methods

Subjects 1, 2 and 3 are Jordanian siblings from non-consanguineous healthy parents (Fig. 1). Subjects 1 and 2 are male, while subject 3 is female. Subjects 2 and 3 are dizygotic twins. Pertinent clinical findings are summarized in the Table 1. Subject 1 was prenatally diagnosed with hydronephrosis, hydroureters, and polyhydramnios. He was delivered at 37 weeks by caesarian section because of macrosomia and weighed 3920 g. A diagnosis of SGBS was suspected in the neonatal period because of prenatal onset of overgrowth and physical features including

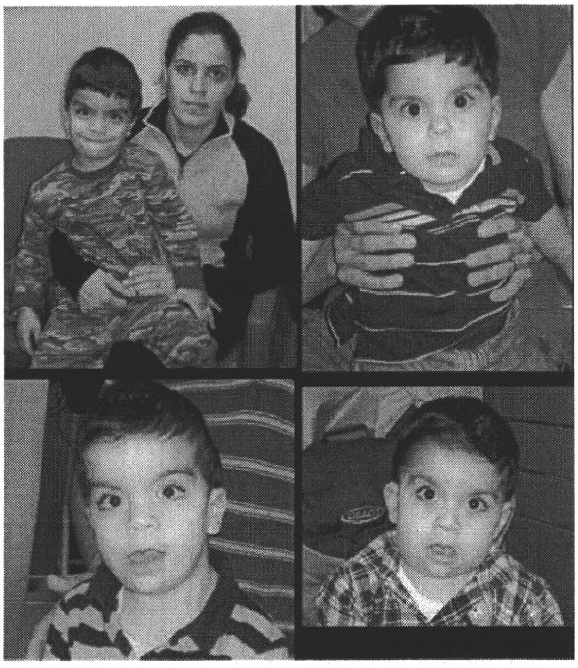

*Fig. 1.* Upper left: photos of Subject 1 (30 months) and Subject 4 (26 years); Upper right: photo of Subject 3 (12 months); Lower left: photo of Subject 1 (25 months); Lower right: photo of Subject 2 (12 months).

down-slanting palpebral fissures, prominent ala nasi, prominent metopic suture, macroglossia, mild pectus excavatum, large feet and hands and skeletal anomalies with 13 ribs. DNA sequence analyses of *GPC3* revealed a mutation of c.256C>T (p.Arg86X) confirming the diagnosis. His motor and speech development have been delayed: walking at 15 months and <10 words vocabulary at 25 months. Subject 2 was born at 34 weeks gestation by caesarian section. He weighed 3710 g (>97th percentile on the adjusted preterm growth chart). He was also diagnosed prenatally with hydronephrosis, hydroureters, and macrocephaly/macrosomia, and skeletal survey at birth showed abnormal chest cage with 13 ribs. At 3 months of age, he had mild scaphocephaly, characteristic facies with proptotic and prominent eyes, prominent ala nasi and up-turned nose and mild pectus excavatum. X-ray studies at 12 months showed advanced bone age equivalent to 16 months. His development has been delayed: he could not walk independently and had four single words at 17 months. The same mutation of c.256C>T (p.Arg86X) was identified in *GPC3*. Subject 3 is a female, the dizygotic twin sister of subject 2. She weighed 2196 g at birth (below the 50th percentile for weight). She was diagnosed with a congenital diaphragmatic hernia that was surgically repaired in the neonatal period.

Table 1. Summary of clinical findings

| Sb. 1 Male | Sb. 2 Male | Sb. 3 Female | Sb. 4 Female | Clinical findings |
|---|---|---|---|---|
| (37 weeks) | (34 weeks) | (34 weeks) | FT | At birth (gestational age) |
| + | + | – | | Macrosomia |
| 3920 g | 3710 g | 2195 g | unk | Birth weight |
| – | – | – | – | Craniofacial |
| + | + | + | – | Macrocephaly |
| + | + | + | + mild | Coarse face |
| + | + | – | – | Ocular hypertelorism |
| + | + | – | – | Epicanthal folds |
| + | + | – | – | Thick auricles |
| + | + | + | – | Wide nasal bridge and anteverted nares |
| + | + | – | + mild | Macrostomia/macroglossia |
| + | + | – | – | Midline groove in the lower lip and/or deep furrow in the middle of the tongue |
| + | + | – | – | High arched/narrow palate |
| – | – | – | – | Hands |
| + | + | – | – | Large hands |
| – | – | – | – | Postaxial polydactyly |
| – | – | – | – | Chest/abdomen |
| – | – | – | – | Supernumerary nipples |
| + | + | – | – | Pectus excavatum |
| + | + | – | – | Rib/vertebral abnormalities |
| + | + | – | – | Umbilical/inguinal hernias |
| – | – | – | – | Genitalia |
| + | – | | | Hydrocele |
| – | – | – | – | Internal organs |
| + | – | + | – | Congenital heart defect |
| VSD | – | PDA | – | (VSD: ventricular septal defect, PDA: patent ductus arteriosus) |
| – | – | + | – | Diaphragmatic hernia |
| + | + | – | – | Hepatomegaly |
| – | – | + | – | Cystic dysplasia of kidneys |
| + | + | – | – | Nephromegaly |
| + | + | – | – | Hydronephrosis |
| – | + | – | – | Hydroureter |
| – | – | – | – | Neurological findings |
| + | + | – | – | Speech delay |
| + | + | + | – | Motor delay |
| – | – | – | – | Other findings |
| + | – | + | – | Vertebral anomalies |
| + | + | – | – | Advanced bone age |

FT, full term; unk, unknown; Sb, subject; Sb2 and 3 are dizigotic twins.

Ultrasound studies showed a small patent ductus arteriosus (PDA) and small cystic lesions in the left kidney. She had a developmental evaluation at the age of 5 months which revealed fine motor delay. At the age of 3 months, her height, weight and occipito-frontal circumference were at the 10th, 25th, and 25th percentile, respectively. However, by 8 months of age all the measurements were above the 90th percentile. Although, her facial features were not typical for SGBS, developmental delay and dysmorphic features including macrocephaly, PDA and congenital diaphragmatic hernia strongly suggested SGBS. Subject 4 is their mother. She has normal intelligence, and is in good health. She has very mild clinical signs such as slight coarse facies and macrostomia. Subjects 3 and 4 were tested for *GPC3* mutations, which revealed the heterozygous mutation of c.256C>T (p.Arg86X).

## Methods

Assays for the analyses of X-chromosome inactivation were performed using genomic DNA extracted from peripheral blood, buccal swabs, and cultured skin fibroblasts in the two female

individuals with the mutation in *GPC3*. The X-chromosome inactivation status was evaluated by the following two methods: the analysis of the CAG repeats in the human androgen-receptor gene (*AR*) at Xq11-q12 following the method described by Allen et al. (13) and the analysis of the CCG repeats in the 5′-untranslated region of the Fragile XE (*FRAXE*) gene at Xq28 using forward: 5′-GCGAGGAAGCGGCGGCAGTGGCACTGGG-3′ and reverse: 5′-CCTGTGAGTGTGTAAGTGT GTGATGCTGCCG-3′ primers following the same protocol as above. [University of Southern California Health Science Campus Institutional Review Board approved (ethics approval) the study.]

## Results

Analysis of *AR* indicated that the mother had homozygous alleles with 21 CAG repeats and subject 3 received an X-chromosome containing the 21 CAG repeats allele from the mother and the 22 repeats allele from the father. The studies in subject 3 revealed that the X-inactivation ratio was 21 (20%) : 22 (80%).

The result indicates that paternal X-chromosome ($n = 22$ repeats) was preferentially inactivated in subject 3 and the studies were not informative for the mother. Analysis of *FRAXE* indicated that the mother had an allele with 14 (CCG) repeats and an allele with 20 repeats. The X-inactivation ratio was 14 (57%) : 20 (43%). Subject 3 received an allele with 14 repeats from the mother and the other with 17 repeats from the father. The X-inactivation ratio was 14 (29%) : 17 (71%). This indicates that the X-chromosome with the mutation was inactivated by 57% in the mother (subject 4) and by 29% in her affected daughter (subject 3). The study results with buccal swabs and cultured skin fibroblasts specimens were quite different from the ones with blood specimens (Table 2). Analysis of *AR* with skin fibroblasts showed that the X-inactivation ratio was 21 (72%) : 22 (28%) in subject 3. Analysis of *FRAXE* with skin fibroblasts showed the ratio of 14 (77%) : 17 (23%) in subject 3 and 14 (70%) : 20 (30%) in subject 4. Analysis of FRAXE with buccal swabs specimens showed the ratio of 14 (44%) : 17 (56%) in subject 3 and 14 (42%) : 20 (58%) in subject 4.

Table 2. Analysis of X-inactivation by the androgen receptor (*AR*) and the fragile XE (*FRAXE*) loci

| Gene | Specimen | Subject 3 | | Subject 4 | |
|---|---|---|---|---|---|
| *AR* | (Repeats) | (21) | (22) | (21) | (21) |
| | Blood, $n = 2$ | 20 | 80 | n/a | n/a |
| | Fibroblasts, $n = 2$ | 72 | 28 | n/a | n/a |
| *FRAXE* | (Repeats) | (14) | (17) | (14) | (20) |
| | Blood, $n = 3$ | 29 SD: 2 | 71 | 57 SD: 3.6 | 43 |
| | Fibroblasts, $n = 3$ | 77 SD: 1 | 23 | 70 SD: 8.4 | 30 |
| | Buccal swabs | 44 | 56 | 42 | 58 |

Subject 4 was homozygous for the repeats at *AR*.
*n*, number of repeated assay; n/a, not applicable; SD, standard deviation.

## Discussion

SGBS is an X-linked condition and mutations in *GPC3* at Xq26 are known to be responsible to cause SGBS (7). *GPC3* encodes the glypican-3 protein which is thought to play an important role in growth control in embryonic mesoderm derived tissues (7). Although, *GPC3* is highly expressed in mesodermal embryonic tissues including liver, lung, and kidney, it is expressed neither in the fetal brain tissue nor in skin fibroblasts as they are formed from the ectoderm. The studies were conducted with blood, buccal swabs and skin fibroblasts. Only the studies with blood cells could show moderately skewed X-inactivation in the affected daughter (subject 3) with the ratio of inactivation of the X-chromosome without the mutation by 71–80%. Her mother with mild symptoms (subject 4) did not show skewed X-inactivation with blood specimens. As *GPC3* has tissue specific expressions and is not one of the housekeeping genes, it is not expressed in the ectodermal cells. Skin fibroblasts and buccal swabs may not be suitable specimens to study the effects of *GPC3* mutation because of skewed X-inactivation. Blood cells and internal organs including lung, liver and kidney are formed from the mesoderm. Although, *GPC3* is minimally expressed in adult tissues, the profile of X-inactivation should remain the same from the embryo stage (7). As analyses of X-inactivation with internal organs are impractical, blood is likely the most appropriate specimen that possibly reflects abnormal *GPC3* functions at embryonic stage because of skewed X-inactivation.

X-linked disorders affect males, where as female carriers are generally spared. This is thought to be because of the random inactivation in females of one of the two X-chromosomes in all somatic cells (14). Only a few female patients with mild expressions of the SGBS phenotype have been reported (2, 11). A female with typical SGBS with an X-autosome translocation has been reported by Punnett (12). An X-autosome translocation is known to cause skewing effects because of the selection for survival advantage (15). Approximately 10% of the population

shows skewing as extreme as 90/10 by random X-inactivation (16). On the basis of these observations, it is thought that the effect of Lyonization is the underlining mechanism for female carriers to have a milder phenotype. The X-chromosome inactivation studies in the presented family showed that predominant expression of the X-chromosome with the *GPC3* mutation in subject 3 and predominant expression of the normal X-chromosome in the mother with mild symptoms (Subject 4). It is unclear why there is 9% difference between the two results with *AR* and *FRAXE* in subject 3. This might be reflecting the limitations of accuracy in these X-inactivation studies. Skewed X-inactivation usually means that an allele is preferentially inactivated by >90% (17). As it does not seem to be survival advantage over the cells without the mutation in GPC3, moderate degree of skewed X-inactivation in the subject 3 is likely because of random X-inactivation. The mechanisms leading to a skewed X-inactivation in females with X-linked disorders are reviewed by Puck and Willard (14).

Discordant expression of a few housekeeping genes including hypoxanthine guanine phosphoribosyltransferase (HPRT, EC 2.4.2.8) and alpha-galactosidase A (EC 3.2.1.22) in monozygotic twin pairs with Lesch–Nyhan disease and with Fabry disease, respectively, have been reported (18, 19). In these reports, X-inactivation analyses showed different patterns between blood cells and skin fibroblasts. A skewed pattern was demonstrated in the fibroblasts in the affected twins in these conditions. Although, a hypothesis that the process responsible for monozygotic twinning to lead skewed X-inactivation in monozygous twin sisters may exist, it is probably unlikely for the process to affect the moderately skewed X-inactivation of blood cells in the affected dizygotic twin female subject (subject 3) as chromosome studies with her blood did not show a chimera with 46,XY cells (18). Placental vascular connections occur in 8% of dizygotic twins (20). However, it is unlikely that vascular connections could have any effects on the profile of X-inactivation in subject 3.

In the presented case here, subject 3 showed a moderately skewed X-inactivation (71–80%). Loss of the functional glypican-3 protein by 71–80% degree is appeared to be above the threshold to develop the SGBS phenotype. The X-inactivation studies in the mother showed inactivation of the X-chromosome with the mutation by 57%. This suggests that loss of the functional glypican-3 protein by 43% is slightly above or close to the threshold to develop the SGBS phenotype.

These X-inactivation studies with peripheral blood DNA specimens (mesoderm origin) showed the most reasonable results that can provide explanations for the phenotypic features in the two female subjects. Ectodermal origin of skin fibroblasts and buccal swabs showed the contradicting results against the ones from blood specimens and the two female subjects showed the almost identical X-inactivation patterns. This suggests that it is critical to choose appropriate specimens based on the gene functions and expressions to evaluate if skewed X-inactivation is responsible for clinical findings. Further studies are indicated to disclose correlation of *GPC3* genotypes, the levels of expression, and clinical phenotypes in female individuals with SGBS.

## References


1. Simpson JL, Landey S, New M et al. A previously unrecognized X-linked syndrome of dysmorphia. Birth Defects 1975: 11: 18–24.
2. Golabi M, Rosen L. A new X-linked mental retardation overgrowth syndrome? Am J Med Genet 1984: 17: 345–358.
3. Behmel A, Plochi E, Rosenkranz W. A new X-linked dysplasia gigantism syndrome: identical with the Simpson dysplasia syndrome? Hum Genet 1984: 67: 409–413.
4. Neri G, Marini R, Cappa M et al. Simpson-Golabi-Behmel syndrome: an X-linked encephalo-tropho-schisis syndrome. Am J Med Genet 1988: 30: 287–299.
5. Chen E, Johnson JP, Cox VA et al. Simpson-Golabi-Behmel syndrome: Congenital diaphragmatic hernia and radiologic findings in two patients and follow-up of a previously reported case. Am J Med Genet 1993: 46: 574–578.
6. Li M, Shuman C, Fei YL et al. GPC3 mutation analysis in a spectrum of patients with overgrowth expands the phenotype of Simpson-Golabi-Behmel syndrome. Am J Med Genet 2001: 102: 161–168.
7. Pilia G, Hughes-Benzie RM, Mackenzie A et al. Mutations in GPC3, a glypican gene, cause the Simpson-Golabi-Behmel syndrome. Nat Genet 1996: 12: 241–247.
8. Brzustowicz LM, Farrell S, Khan MB et al. Mapping of a new SGBS locus to chromosome Xp22 in a family with a severe form of Simpson-Golabi-Behmel syndrome. Am J Hum Genet 1999: 65: 779–783.
9. Mariane S, Iughetti L, Bertorelli R et al. Genotype/phenotype correlations of males affected by Simpson-Golabi-Behmel syndrome with GPC3 gene mutations: patient report and review of the literature. J Pediatr Endocrinol Metab 2003: 16: 225–232.
10. Veugelers M, Cat BD, Muyldermans SY et al. Mutation analysis of the GPC3/GPC4 glypican gene cluster on Xq26 in patients with Simpson-Golabi-Behmel syndrome: identification of loss-of-function mutations in the GPC3 gene. Hum Mol Genet 2000: 9: 1321–1328.
11. Behmel A, Plochl E, Rosenkranz W. A new X-linked dysplasia gigantism syndrome: follow up in the first family and report on a second Austrian family. Am J Med Genet 1988: 30: 275–285.
12. Punnett HH. Simpson-Golabi-Behmel Syndrome in a female with an X-autosome translocation. Am J Med Genet 1994: 50: 391–393.
13. Allen RC, Zoghbi HY, Moseley AB et al. Methylation of *Hpa*II and *Hha*I sites near the polymorphic CAG repeat in the

human androgen-receptor gene correlates with X chromosome inactivation. Am J Hum Genet 1992: 51: 1229–1239.
14. Puck JM, Willard HF. X inactivation in females with X-linked disease. N Engl J Med 1998: 338: 325–328.
15. Heard E, Clerc P, Avner P. X chromosome inactivation in mammals. Annu Rev Genet 1997: 31: 571–610.
16. Naumova AK, Plenge RM, Bird LM et al. Heritability of X chromosome inactivation phenotypes in a large family. Am J Hum Genet 1996: 58: 1111–1119.
17. Beever CL, Stephenson MD, Penaherrera MS et al. Skewed X-chromosome inactivation is associated with trisomy in women ascertained on the basis of recurrent spontaneous abortion or chromosomally abnormal pregnancies. Am J Hum Genet 2003: 72: 399–407.
18. De Gregorio L, Jinnah HA, Harris JC et al. Lesch-Nyhan disease in a female with a clinically normal monozygotic twin. Mol Genet Metab 2005: 85: 70–77.
19. Redonnet-Vernhet I, van Amstel JKP, Jansen RPM et al. Uneven X inactivation in a female monozygotic twin pair with Fabry disease and discordant expression of a novel mutation in the alpha-galactosidase A gene. J Med Genet 1996: 33: 682–688.
20. Hall JG. Twinning: mechanism and genetic implications. Curr Opin Genet Dev 1996: 6: 343–347.

# Disrupted *SOX10* Regulation of *GJC2* Transcription Causes Pelizaeus-Merzbacher-Like Disease

Hitoshi Osaka, MD, PhD,[1,2]
Haruka Hamanoue, MD, PhD,[3]
Ryoko Yamamoto, MSc,[4]
Atsuo Nezu, MD, PhD,[5] Megumi Sasaki, BA,[4]
Hirotomo Saitsu, MD, PhD,[3]
Kenji Kurosawa, MD, PhD,[6]
Hiroko Shimbo, MP,[1]
Naomichi Matsumoto, MD, PhD,[3]
and Ken Inoue, MD, PhD[4]

**Mutations in the gap junction protein gamma-2 gene, *GJC2*, cause a central hypomyelinating disorder; Pelizaeus-Merzbacher-like disease (PMLD; MIM311601). Using a homozygosity mapping and positional candidate gene approach, we identified a homozygous mutation (c.-167A>G) within the *GJC2* promoter at a potent SOX10 binding site in a patient with mild PMLD. Functionally, this mutation completely abolished the SOX10 binding and attenuated *GJC2* promoter activity. These findings suggest not only that the *SOX10*-to-*GJC2* transcriptional dysregulation is a cause of PMLD, but also that *GJC2* may be in part responsible for the central hypomyelination caused by *SOX10* mutations.**

ANN NEUROL 2010;68:250–254

Congenital hypomyelinating disorders are a heterogeneous group of central nerve system (CNS) leukoencephalopathies, most of which are inherited disorders of myelin formation. The prototype condition is Pelizaeus-Merzbacher disease (PMD; MIM312080), an X-linked disorder caused by mutations in the proteolipid protein 1 gene (*PLP1*).[1] Patients with PMD have nystagmus, impaired motor development, ataxia, choreoathetotic movements, dysarthria, and progressive spasticity. However, ~20 to 50 % of patients clinically diagnosed with PMD have no detectable abnormalities in the *PLP1* gene, and some have a distinct disease, Pelizaeus-Merzbacher-like disease (PMLD; MIM311601).

Mutations in the gap junction protein gamma-2 gene (*GJC2*, also known as *Cx47* or *GJA12*) have been reported as a cause of PMLD.[2–8] Twenty-four different mutations (8 frameshift, 10 missence, 5 nonsense, and 1 missense/insertion alterations) have been reported to date, and most if not all result in a loss of channel function.[7,9]

By combining homozygosity mapping and a candidate gene approach, we found a homozygous mutation that disrupts a SOX10 transcriptional activation site in the *GJC2* promoter region in a family showing a mild PMLD phenotype. SOX10 is an high mobility group (HMG) family transcription factor that plays a critical role in peripheral nervous system (PNS) and CNS myelination. In addition, a subset of *SOX10* mutations cause peripheral and central hypomyelination, Waardenburg syndrome, and Hirschsprung disease (PCWH; MIM609136).[10] This study reports the first case of PMLD caused by a mutation in the *GJC2* promoter and suggests that *SOX10* transcriptional regulation of *GJC2* plays a critical role in CNS myelination.

## Patients and Methods

Detailed clinical information of a Japanese female patient with PMLD, who is now 25-years-old, was previously reported.[11] In brief, her healthy parents were second cousins. She had congenital pendular nystagmus as a neonate, but otherwise developed normally and was educated at a normal school. At the age of 10 years, she developed a spastic gait that worsened and made her wheelchair bound by the age of 12 years. Her disease progressed to mild athetosis of the upper limbs and ataxia by age 13 years and dysarthria by age 15 years. She cannot speak and understands only easy commands now. Brain magnetic resonance imaging at age 15 and 20 years showed diffuse hyperintensity of white matter on T2-weighted images with interval progression of brain atrophy (Fig 1). Electrophysiological examinations showed extensive nerve conduction slowing in the CNS, although this was less severe than usually seen in male patients with PMD.[11] Peripheral nerve conduction velocities were nor-

From the [1]Division of Neurology, Clinical Research Institute, Kanagawa Children's Medical Center; [2]Molecular Pathology and Genetics Division, Kanagawa Cancer Center Research Institute; [3]Department of Human Genetics, Yokohama City University Graduate School of Medicine; [4]Department of Mental Retardation and Birth Defect Research, National Institute of Neuroscience, National Center of Neurology and Psychiatry, Kodaira; [5]Division of Pediatric Neurology, Yokohama Ryoiku-iryo Center; and [6]Division of Genetics, Clinical Research Institute, Kanagawa Children's Medical Center, Yokohama, Japan.

Address correspondence to Dr Osaka, Division of Neurology, Clinical Research Institute, Kanagawa Children's Medical Center, Yokohama, 232-855, Japan. E-mail: hosaka@kcmc.jp

Additional Supporting Information can be found in the online version of this article.

Received Dec 29, 2009, and in revised form Jan 29, 2010. Accepted for publication Feb 26, 2010.

Published online in Wiley InterScience (www.interscience.wiley.com). DOI: 10.1002/ana.22022

 